Operationally Stable and Efficient $CsPbI_{3-x}Br_x$ Perovskite Nanocrystals Light-Emitting Diodes Enabled by Ammonium Ligand Surface Treatment

Yiyue Zhang[1,2], Lata Chouhan[1], Eduard Fron[1], Luca Leoncino[3], Karim Elkhouly[2], Lotte Clinckemalie[1], Harshita Bhatia[1], Maarten B.J. Roeffaers[4], Weiming Qiu[2,*], Johan Hofkens[1, 5, *], Elke Debroye[1], Bapi Pradhan[1,*]

[1]Molecular Imaging and Photonics, Department of Chemistry, KU Leuven, Celestijnenlaan 200F, Leuven, 3001, Belgium

[2]Imec, Kapeldreef 75, Leuven, 3001, Belgium

[3]Electron Microscopy Facility, Istituto Italiano di Tecnologia, via Morego 30, Genova 16163, Italy

[4]cMACS, Department of Microbial and Molecular Systems, KU Leuven, Celestijnenlaan 200F, 3001 Leuven, Belgium

[5]Max-Planck-Institute for Polymer Research, 55128, Mainz, Germany

*Corresponding author. E-mail: johan.hofkens@kuleuven.be, bapi.pradhan@kuleuven.be, weimingqiu@gmail.com

Abstract

Nanocrystals (NCs) of inorganic lead halide perovskites with narrow emission line widths hold great potential for next-generation color-saturated optoelectronic devices. However, their stability and electroluminescence performance are currently hindered by environment-dependent structure deterioration over time and inferior carrier transport. These limitations are closely related to the surface defect-mediated nonradiative energy losses of the NCs. Herein, we have developed a comprehensive surface optimization strategy for $CsPbI_{3-x}Br_x$ NCs, involving molecular passivation, phase stability optimization, and effective electron transport for constructing a durable device. This results in a high-efficiency perovskite light emitting diode (PeLED) exhibiting red emission with a maximum at 685 nm and an external quantum efficiency (EQE) of up to 12.35%. Furthermore, the optimized device shows a much-improved operational stability with a half-lifetime (T_{50}) of 50 min, which is 7 times higher than the untreated device (T_{50} = 7 min). Additionally, the passivated NCs exhibit non-blinking characteristics at the single-particle level. This work highlights the tremendous potential of amino-rich ligands in stabilizing perovskite NCs for efficient and operationally stable LEDs.

Keywords $CsPbI_{3-x}Br_x$ perovskites, Nanocrystals, Light-emitting diodes, Blinking, Fluorescence upconversion

1. Introduction

Over the past decade, incredible advances have been achieved in improving the performance of all-inorganic lead halide perovskite-based (LHP) optoelectrical devices, including solar cells[1-3], photodetectors[4-5], and light-emitting diodes (LEDs)[6-8]. Among the different forms of LHPs, inorganic nanocrystals (NCs) are emerging as one of the most exciting optoelectronic materials for LED displays by virtue of their ease of solution processability and excellent photophysical properties, such as substantially decreased defect density[9], high photoluminescence quantum yield (PLQY), and narrow full-width at half-maximum (FWHM, ~35 nm) emission bands [10-14]. Other competing materials, such as organic fluorophores, typically show broader emission line widths (FWHM > 60 nm) and low brightness, hence resulting in LEDs with inferior color purity [15]. Due to the advancement in material engineering of perovskite NCs in terms of morphology, stoichiometric control, and surface treatment, the highest external quantum efficiency (EQE) reported is 23.4% for green PeLEDs based on $CsPbBr_3$/MABr (MA: methylammonium) quasi-core/shell structures[16] and 23.0% for red PeLEDs based on $CsPbI_3$[17]. However, the operational stability as well as color tunability of such devices, particularly for the red PeLEDs, require further improvement.

$CsPbI_{3-x}Br_x$ NCs have gained significant attention as the most promising material in the inorganic perovskite NCs family[18]. Nonetheless, there are still several challenges in the practical operation of $CsPbI_{3-x}Br_x$ NC-based LEDs, such as: (i) the operating voltage of NC LEDs is elevated by spatially confined electrons and holes in the NCs, which limits the carrier transport among different NCs to efficiently form excitons [19-20]. This becomes more profound when the surface area of the small-size NCs is wrapped with a massive amount of surface ligands from the colloidal synthesis, forming an insulating layer around the NCs. (ii) pure $CsPbI_3$ perovskite suffers from prominent phase instability problems since it readily transforms from metastable black phase to yellow phase at room temperature, thereby reducing the operational stability of the fabricated LEDs[19, 21-24]. (iii) There are still major defect-mediated nonradiative energy losses, mainly at the perovskite NCs surface[9]. Therefore, finding methods to effectively suppress the defects and enhance phase stability of the $CsPbI_{3-x}Br_x$ NCs is a key target to realize the desirable performance of PeLEDs for practical applications.

Surface ligands are crucial for maintaining the crystal phase and optical properties of LHP NCs[23, 25], and therefore NCs are typically synthesized in the presence of high concentrations of ligands. After the complete growth of the NCs, an optimum anti-solvent washing step is required to remove the excess surface ligands from the surface without destroying colloidal dispersion stability. However, after purification, the ionic nature of LHPs and non-neglectable dynamics of the binding ligands often result in a large number of ionic vacancy defects on the surface of perovskite NCs[7, 26-27]. To mitigate this issue, various surface post-treatment strategies using small organic molecules or metal cations have been applied to passivate surface defects and optimize the performance of perovskite NCs[19, 23, 28-31]. For example, red PeLEDs based on $CsPbI_{3-x}Br_x$ NCs having an EQE of up to 23% were recently demonstrated by applying potassium iodide surface passivation[17]. A variety of monovalent (in)organic cations can be used to passivate the dangling bonds on the surface of LHP NCs.

In contrast to small inorganic ions, small organic molecules can avoid the use of highly polar solvents in the passivation process[17]. This is important because such polar solvents can lead to additional defects or even alter the structure and morphology of perovskite NCs[15, 18, 32]. Among the different organic cations, guanidinium (GA) is a highly stable small organic cation exhibiting an effective resonance stability of three amino groups. Previous reports have shown that due to the additional hydrogen bonding via its amino group, GA can simultaneously stabilize the surface and improve charge carrier transport in perovskites with alternating cations in the interlayer space (ACI)[33-34]. From this, the application of NC-based GA surface passivation of PeLEDs would be potential.

This work demonstrates a facile surface passivation strategy of $CsPbI_{3-x}Br_x$ NCs by introducing guanidinium iodide (GAI) to fabricate stable red emitting PeLEDs. The obtained GAI-passivated NCs exhibit high brightness, high dispersibility, non-blinking at a single-particle level, and good stability for months under ambient conditions. Bright red PeLEDs fabricated using those NCs displayed an impressive EQE of 12.35% at a low turn-on voltage close to 2.4V, and a maximum luminance of 4624 cd/m^2, with a peak electroluminescence at 685 nm. The operational half-life T_{50} of the GAI-treated device was 50 mins at the current density of 20 mA/cm^2, which is superior to the untreated device under the same conditions. Furthermore, PL blinking at the single particle level is well suppressed for GAI-passivated NCs, indicating that passivation reduces random switching between different PL intensity states, suggesting effective passivation of defects acting as charge traps, which results in the improved performance of the PeLED.

2. Results and Discussion

$CsPbI_3$ perovskite NCs are usually synthesized with OA and OAm ligands at high temperatures and purified with MeOAc. These $CsPbI_3$ NCs readily transform from the photoactive black phase to a non-perovskite yellow phase. Incorporating Br into I-based perovskites is a common strategy to stabilize the $CsPbI_3$ structure[29, 35]. In most cases, $PbBr_2$ is introduced into the reaction mixture as a bromine dopant source, leading to the synthesis of $CsPbI_{3-x}Br_x$. However, these I:Br mixed perovskites exhibit irreversible phase separation caused by the migration of halide ions under variable environmental conditions (temperature, humidity, and voltage bias) during further device applications[10, 29, 36-38]. In this study, we refer to the earlier optimized synthesis of nanocrystalline hexagonal $CsPbBr_3$ by introducing phenacyl bromide as a source of bromine[14]. This strategy includes increasing the PbI_2 dissolution temperature to 220 °C, followed by the injection of 2 ml OAm. After the reaction is carried out for 20 mins, the temperature of the system is lowered to 150°C until the solution becomes transparent. The Cs-oleate precursor is then rapidly injected when the solution temperature reaches 170 °C, to synthesize high-quality stable $CsPbI_{3-x}Br_x$ NCs. The Br doping by this method is anticipated to promote the crystal grain growth and enhance the phase stability with little impact on the absorption features (bandgap, oscillator strength) [14]. The stability of NCs under environmental conditions is improved by synthesizing high-quality NCs and limiting the amount of bromine to minimize ion migration in the NCs.

After purification by simple centrifugation, we introduce GAI into the NCs. We have performed the surface treatment in octane to stabilize the surface of the NCs and purify them without damaging their octahedral structure or changing the quantum confinement effect. The pristine sample began to transform to the non-perovskite phase within 2 days under ambient condition storage (Figure S1). In contrast, we observed that the $CsPbI_{3-x}Br_x$ NCs solution is more robust after adding GAI (Figure S2). Investigation of the change in the colour of NCs showed that an excess (50 µL) of GAI or Br doping (more than 5%) would cause the colour of the NCs solution to lighten rapidly (Figure S3). Here, we chose the sample with the best performance and stability for further processing, being the NC sample with the addition of 5% Br and 20 µL of GAI solution.

Figure 1a shows the X-ray diffraction (XRD) pattern of the 3 samples (pure $CsPbI_3$ NCs, $CsPbI_{2.85}Br_{0.15}$ NCs, and GAI-passivated $CsPbI_{2.85}Br_{0.15}$ NCs), which all match the cubic references of bulk $CsPbI_3$ [19, 22, 39-40]. In the XRD pattern of pure $CsPbI_3$, in addition to α-$CsPbI_3$, a small amount of δ-$CsPbI_3$ is observed, which may be due to the poor stability of α-$CsPbI_3$ in the non-treated sample. Phase transition might have occurred during the data recording of the XRD experiment. It is reported that the NCs stability is closely associated with the phase structure, with a stability sequence of cubic (α-phase) < tetragonal (β-phase) < orthorhombic (γ-phase) < yellow phase (δ-phase)[40]. This was not observed in either CPIB or GAI-CPIB. As seen in Figure 1a, all the NCs exhibit the featured diffraction peaks at 14.7 and 28.6°, typically belonging to the (100) and (200) planes of cubic perovskite crystals, respectively. The intense diffraction peaks of the (100) and (200) planes indicate that the perovskite NC

films are highly crystalline and preferably orientated along (l00) directions. The XRD peaks of the $CsPbI_{3-x}Br_x$ NC films gradually shifted to higher angles upon adding Br in the precursor. Since the ionic radius of Br^- is smaller than that of I^-, upon increasing the Br content, the unit cell parameters of the $CsPbI_{3-x}Br_x$ crystal thin film increase[29]. According to Bragg's law, the diffraction peak shifts to a larger angle. Interestingly, adding GAI significantly enhances the intensity of the diffraction peak representing the (100) crystal plane, indicating improved crystallinity. As such, we infer the passivation of GAI may not only fill the empty lattice sites existing at, or near the surface, thereby passivating defect sites. GAI can even affect shrinking the lattice spacing, simultaneously providing strain and thus increasing the crystallinity and stability of $CsPbI_{3-x}Br_x$ NCs[24]. Detailed investigations through high-resolution X-ray diffraction and scattering measurements would enable to quantify these parameters, however, these are out of scope for this study.

To further understand the GA binding motifs on the $CsPbI_{3-x}Br_x$ NCs surface, FTIR spectroscopy was performed to investigate the surface chemistry of the NCs. As shown in Figure 2b, the same vibration bands, including COO^- stretching and C=C−H stretching (1546 cm^{-1}), appear in all three samples, indicating that the OAm ligand was still adsorbed on the NCs surface. GAI binding is evident based on the emergence of FTIR peaks at wavenumbers 3340 and 1662 cm^{-1} that are present in the spectra for GAI and the NCs stabilized with GAI (Figure S4), which can be assigned to the $-NH_2$ symmetric and −C=N stretching vibrations, respectively[41]. Meanwhile, the peak intensity increases proportionally with increasing GA incorporation. The peaks at 2850-2950 cm^{-1} correspond to functional groups in the C-H stretching mode of the ligand. Due to the low concentration of GAI in the precursor, only slightly enhanced peaks representing GAI can be seen. All the above observations suggest that GAI interacts with NCs surface.

Next, to understand the effect of GAI passivation on the morphology of $CsPbI_{3-x}Br_x$ NCs, transmission electron microscopy (TEM) was conducted. BF-TEM images (Figure 1c-d) show that non-GAI-passivated and GAI-passivated NCs adopt a cubic shape with an edge length of (7 ± 2) nm and (7 ± 1) nm, respectively. As expected, the original $CsPbI_3$ solution showed relatively poor stability under ambient conditions. We observed that $CsPbI_{2.85}Br_{0.15}$ at the time of 14 days of aging had aggregated and fused into large particles of several hundreds of nanometers (Figure S6). This typically occurs when $CsPbI_{3-x}Br_x$ based NCs are stored for long periods. Under the same storage conditions, the passivated NCs remained as dispersed cubic particles and retained their black phase. The GAI-passivated NCs exhibit much-enhanced morphology and crystallinity stability after long-term storage.

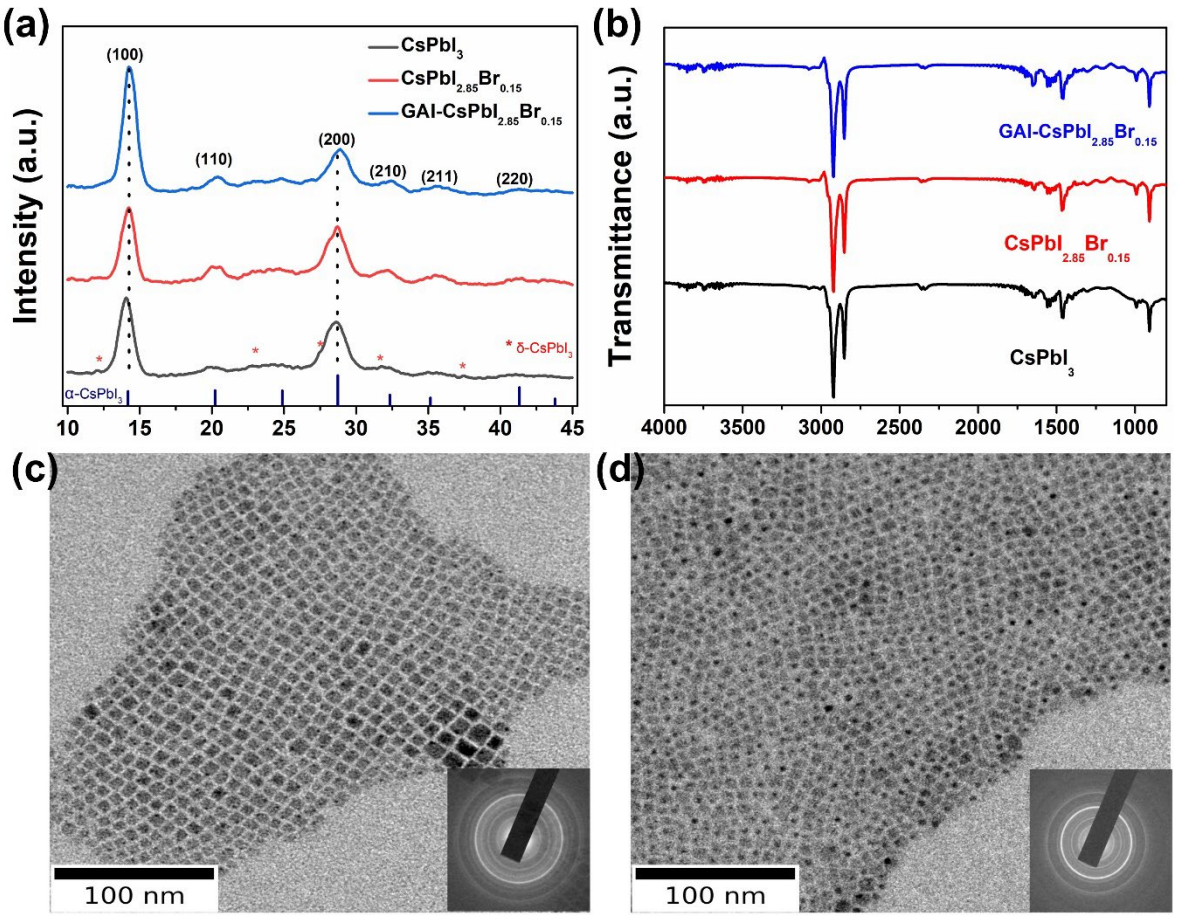

Figure 1. Guanidinium treatment of ~7 nm $CsPbI_{2.85}Br_{0.15}$ QDs and corresponding characterization. **(a)** XRD patterns and (**b)** FTIR spectra of pristine $CsPbI_3$, $CsPbI_{2.85}Br_{0.15}$, and GAI-$CsPbI_{2.85}Br_{0.15}$ NCs. (details in Fig S4) The standard cubic-phase α-$CsPbI_3$ XRD pattern is obtained from ICSD No. 181288. **(c)–(d)** BF-TEM images of the (c) $CsPbI_{2.85}Br_{0.15}$ and (d) GAI-$CsPbI_{2.85}Br_{0.15}$ NCs showing their morphology (inset: the SAED pattern of the corresponding sample, showing crystal structure information, details in Figure S5)

Figure 2a depicts the PL and UV-vis absorbance of $CsPbI_3$, $CsPbI_{2.85}Br_{0.15}$, and GAI-passivated $CsPbI_{2.85}Br_{0.15}$ NCs. All the samples show a similar onset absorption wavelength of around ~665 nm, resulting from the strong quantum confinement effect induced by the reasonably small particle size (exciton Bohr diameter of $CsPbI_3$ is 12 nm)[13]. Hence, the tiny amount of Br doping and GAI passivation did not change the bandgap of the $CsPbI_3$ NCs. It can be observed that Br doping leads to a blue shift of the PL peak, which is consistent with previously reported spectral findings. A small amount of Br doping does not profoundly change the structure of $CsPbI_3$ NCs, but only helps to reduce the surface defects and thus enhance the stability of the NCs in the ambient environment[24, 35, 42-43]. With further surface treatment by adding GAI, a tiny but clear blue shift in PL (about 2 nm) can be observed, which supports the notion of improved crystallinity within the GAI passivated $CsPbI_{2.85}Br_{0.15}$ NCs[41, 44].

Femtosecond fluorescence upconversion measurements were carried out to elucidate the photo-induced exciton generation and consecutive relaxation processes (Figure 2b). For both $CsPbI_{2.85}Br_{0.15}$, and GAI-$CsPbI_{2.85}Br_{0.15}$ NCs, we detect a fast rise followed by two decay components within the 60 ps detection window at the detection wavelength of 680 nm. The time constants are 3.5 ps, 4.5 ps, 26 ps for the $CsPbI_3$ NCs, 3.2 ps, 7.6 ps, 38 ps for the $CsPbI_{2.85}Br_{0.15}$ NCs and 3.6 ps, 4 ps, 19 ps

for the GAI-$CsPbI_{2.85}Br_{0.15}$ NCs, respectively. The fast components (3.5, 3.2 and 3.6 ps) can be attributed to exciton formation whereas the slower ones indicate relaxation and exciton recombination processes. Hence, exciton generation, relaxation and recombination processes are closely related for both samples and not significantly vary within this time scale. The longer exciton decay and free carrier-related radiative recombination are more precisely monitored at longer time scales.

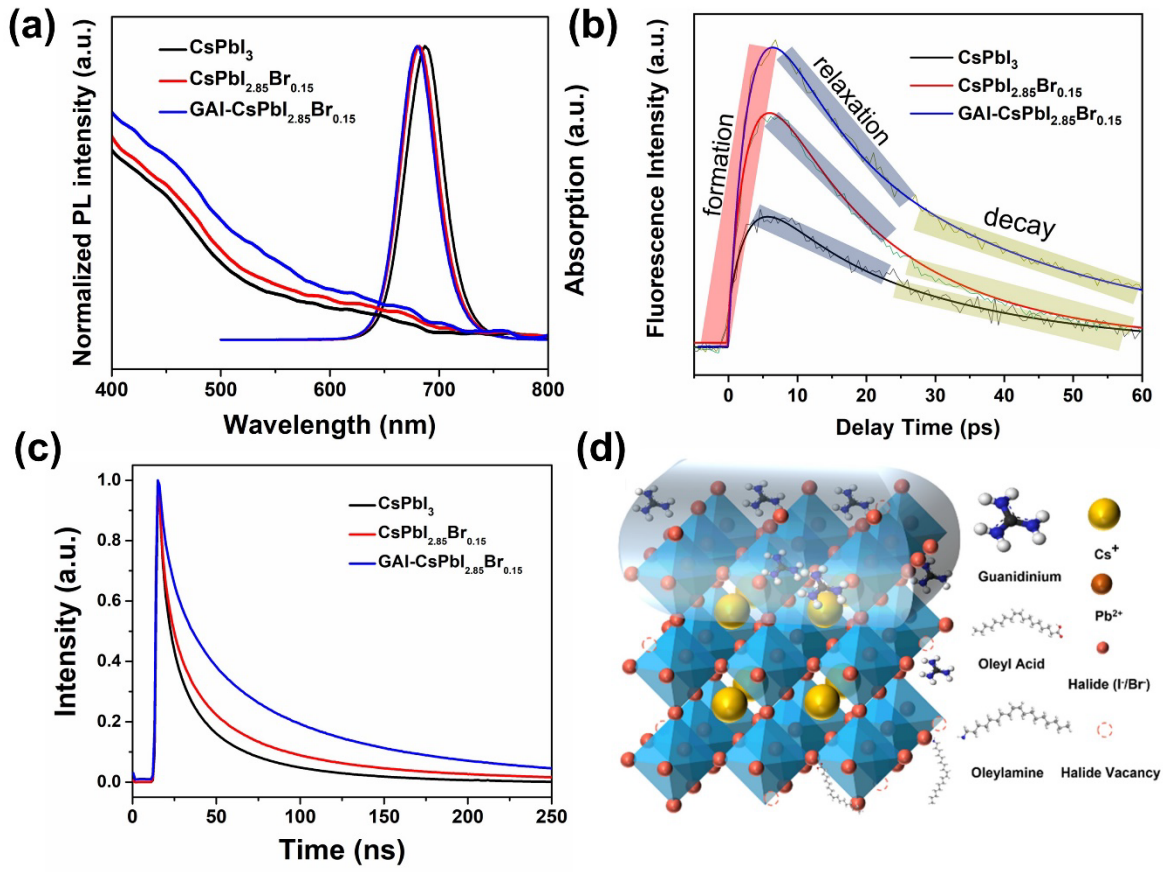

Figure 2. (**a)** PL, and UV-*vis* characterizations, (**b)** Femtosecond fluorescence upconversion measurements, (**c)** TRPL decays of pristine $CsPbI_3$, $CsPbI_{2.85}Br_{0.15}$ and GAI-$CsPbI_{2.85}Br_{0.15}$ NCs. (**d)** Schematic illustration of the passivation of surface defect sites by the GA cation.

Time-resolved PL measurements of $CsPbI_3$, $CsPbI_{2.85}Br_{0.15}$, and GAI-$CsPbI_{2.85}Br_{0.15}$ NCs were measured (Figure 2c) over the ps-ns time scale, as these strongly correlate with the charge carrier diffusion dynamics and recorded efficiency of the LED devices (see last section). In fact, the PL decay time is related to many factors, such as crystal size, crystal shape, related excited state process, defect types, and defect density. Clearly, for defects that promote nonradiative recombination, lower defect densities favour longer lifetimes[45]. PL lifetime information has been extracted by fitting the decay curves using a tri-exponential function. The parameters obtained from the TRPL fit are shown in Table S1. The PL decay of pristine $CsPbI_3$ and $CsPbI_{2.85}Br_{0.15}$ perovskite samples was faster compared to the GAI-treated samples. The amplitude-averaged lifetimes of pristine $CsPbI_3$ and $CsPbI_{2.85}Br_{0.15}$ samples were obtained by numerically integrating the decay curves and were at 14.22 ns and 19.01 ns, respectively, while for GAI-$CsPbI_{2.85}Br_{0.15}$ sample, this value was 20.55 ns. Furthermore, the τ_3 value of the GAI-passivated sample is nearly two times higher than that of the pure $CsPbI_3$ sample (108.67 ns vs 57 ns). This is presumably due to fact that the GAI treatment effectively suppresses the surface defects associated with free charge carrier trapping,

thereby reducing the defect-induced nonradiative decay and increasing the efficiency of the radiative rate processes[46]. A long diffusion length of the free charge carriers is beneficial for uniform charge injection throughout LED devices. A similar phenomenon was reported for $CsPbI_3$ passivated by potassium iodide[17] and phenacyl ammonium iodide[39]. It was found that, following passivation, the average lifetime increases, a higher contribution of the longer lifetime results from an increased number of free charge carriers, indicating a strongly suppressed defect-assisted non-radiative recombination.

PL lifetime components are associated to different photophysical origins across different time scales. The shorter components (ps-ns) are associated with the exciton formation and relaxation processes, and the intermediate lifetimes (ns) are assigned to the radiative recombination decay of excitons. Longer lifetime components (ns-µs) are linked to radiative and nonradiative recombination of free carriers (electron/hole) through defect trapping in the material[17, 47]. From the above, it can be shown that there are a large number of trap-related defects in the pristine $CsPbI_3$ NCs samples. The presence of these defects is partly reduced by Br doping and, notably, can be efficiently passivated by introducing GAI. Guanidinium cations are expected to exist on the surface as shown in Figure 2d. Both positively charged cation and negatively charged anion vacancy defects exist in NCs. GA^+ compensates for the defects on the NCs surface by interacting with surface vacancies/undercoordinated halide ions and generates hydrogen bonds by interacting with undercoordinated Pb^{2+} at the NC surface[41-42, 44, 48]. The hydrogen bonds attract additional halide ions (iodide) to stabilize the structure. Meanwhile, the halide ions lost in the preparation process can also be compensated by the iodide ions of GAI. Therefore, complete defect passivation is essential to achieving the high-efficiency LEDs as described in this study.

To further support the above results and hypothesis on the suppression of nonradiative recombination pathways after post-synthetic treatment of $CsPbI_{2.85}Br_{0.15}$ with GAI, we examined single-particle PL blinking in the NCs. The investigation of PL blinking traces is a reliable method to explore the charge carrier dynamics in perovskite single particles[49-51]. In general, PL blinking is the phenomenon that the PL intensity switches between a bright, neutral state (weak PL quenching = “ON” state) and a charged state (strong PL quenching = “OFF” state) [52-56]. In other terms, PL blinking is attributed to switching between radiative (ON) and nonradiative (OFF) states.

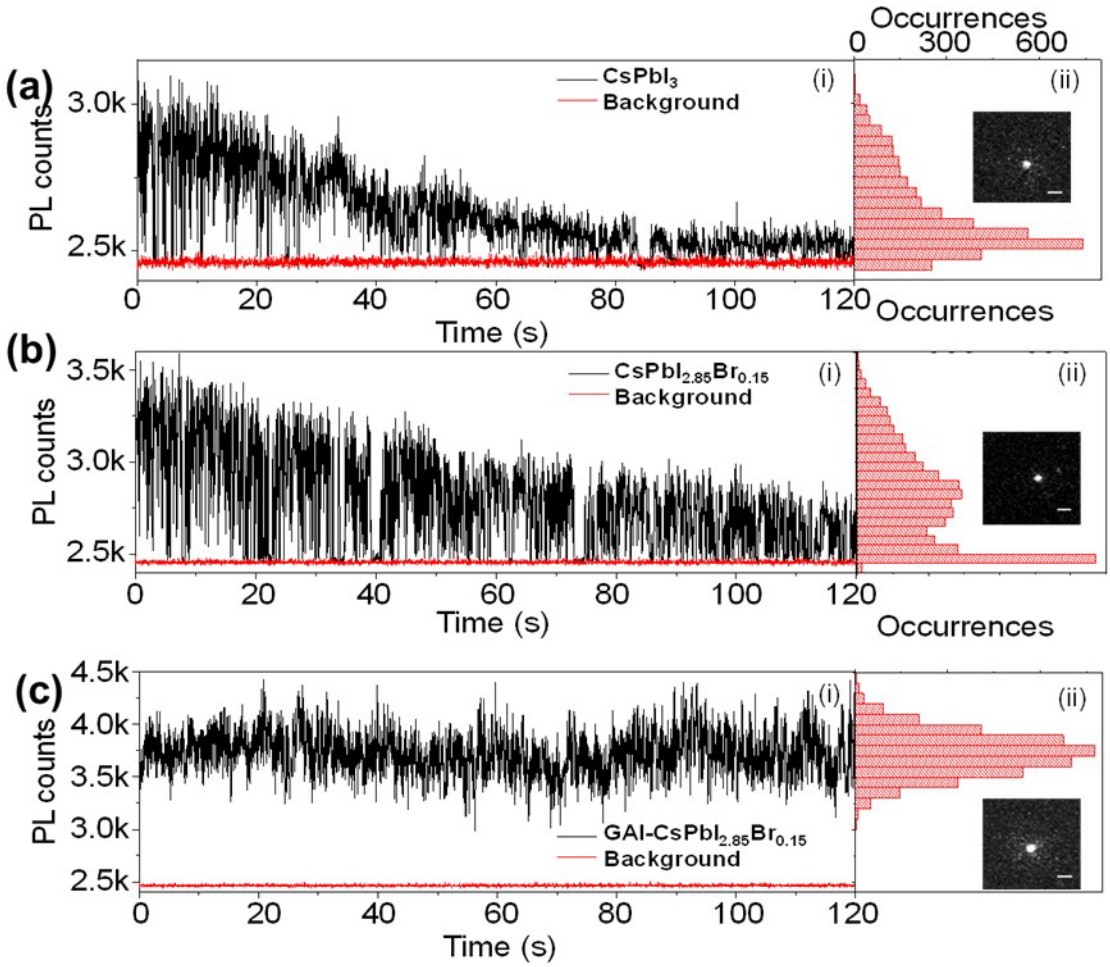

Figure 3. Single-particle PL blinking. (**i**) Representative PL intensity trajectory and (**ii**) corresponding PL intensity occurrences of (**a)** single $CsPbI_3$ NC, (**b)** single $CsPbI_{2.85}Br_{0.15}$ NC and (**c)** single GAI-$CsPbI_{2.85}Br_{0.15}$ NC with their respective background. Inset: The PL images of corresponding NCs collected from the EMCCD camera, scale bar: 1 µm. The excitation power intensity of the 561 nm laser was 0.28 mW cm^{-2} for (a) and 90 µW cm^{-2} for (b) and (c).

Defect activities that strongly influence charge carrier dynamics can be revealed by analyzing the PL blinking data from individual particles. Here, we anticipate understanding the influence of GA^+ post-treatment on individual particles by monitoring PL intensity trajectories (Figure 3). We examined more than 100 single-particle PL trajectories of $CsPbI_3$ NCs with and without GA^+ post-treatment. Firstly, we observed single particles of $CsPbI_3$ NCs in the 55 µm x 55 µm field of view. A representable PL intensity trajectory is shown in Figure 3a (i). In $CsPbI_3$ NCs, we observed fast and random PL blinking with a gradual decrease in PL intensity. The gradual decrease and low PL intensity are due to the degradation of $CsPbI_3$ NCs[57]. We found similar characteristics in non-GAI-treated $CsPbI_{2.85}Br_{0.15}$ NCs (Figure 3b(i), Figure S7). Then, we examined single-particle PL blinking of $CsPbI_{2.85}Br_{0.15}$ NCs treated with GAI (Figure 3c (i)). In this experiment, we observed that the switching between the "ON" and "OFF" states of some particles was inhibited, and a more stable blinking trace could be observed. Furthermore, there is no gradual decrease in the PL intensity in passivated NCs, at least not within the time window of the PL intensity transients that have been collected (120 s), suggesting increased stability of light-induced perovskite degradation. In addition, compare with pure $CsPbI_3$ and $CsPbI_{2.85}Br_{0.15}$ occurrences plot (Figure 3a (ii), 3b (ii)), the PL intensities of GAI-$CsPbI_{2.85}Br_{0.15}$ NCs are primarily in the higher intensity region (Figure 3c (ii)), which suggests the improvement in the PL brightness with the passivation of GAI. Although the effect of GAI on individual NCs requires further research, our work

provides direct evidence that GAI surface passivation is effective in obtaining defect-suppressed $CsPbI_{3-x}Br_x$ NCs. This can offer a particle-level reference for future mechanistic studies of surface passivation.

We next fabricated LED devices using $CsPbI_3$, $CsPbI_{2.85}Br_{0.15}$, and GAI- $CsPbI_{2.85}Br_{0.15}$ NCs films as emitting layers, respectively, to explore how the phenacyl bromide doping and GAI passivation influence the LED performance and stability. The device configuration was ITO/PEDOT: PSS/PVK/ $CsPbI_{3-x}Br_x$ NCs/PO-T2T/LiF/Al and the corresponding schematic of the energy level diagram is illustrated in Figure 4a. The bandgap widths of three perovskite NCs samples are calculated theoretically by Tauc Plot (Figure S10). The normalized EL spectra in Figure 4b are about 5 nm red-shifted relative to the PL spectra potentially owing to the dielectric dispersion of the solvent[58]. Furthermore, in a PeLED, the existence of a multi-layer optical stack modifies the EL peak position compared to a standalone film. Under different applied voltages, GAI-$CsPbI_{2.85}Br_{0.15}$ PeLEDs exhibit stable spectra, and no extra emission can be observed from the carrier transport layers of PEDOT: PSS or PVK, indicating that the injected carriers effectively radiatively recombine in the NCs emission layer. The LEDs with GAI-$CsPbI_{2.85}Br_{0.15}$ NCs exhibit a pure deep red EL emission with a maximum at 685 nm and a FWHM of 30 nm (Figure 4b). This implies that the GAI treatment partly affects the electronic band structure of $CsPbI_{2.85}Br_{0.15}$ NCs presumably due to the change in the perovskite structure following surface passivation of the NCs.

The current density-voltage (J-V) and luminance-voltage (L-V) curves of the LEDs based on the three investigated samples are presented in Figure 4c. All three devices show a low turn-on voltage when the luminance exceeds 1 cd m^{-2} . The relatively low turn-on voltage (3.35 V) of the GAI-$CsPbI_{2.85}Br_{0.15}$ NCs-based LED indicates that the treatment of GAI is beneficial for the efficient charge injection into the emitting layers and enhanced electronic conductivity within close-packed films. In particular, the LED-based on GAI-$CsPbI_{2.85}Br_{0.15}$ NCs exhibited a much higher luminance with a maximum of 4624 cd/m^2 at an applied voltage of 8V. In contrast, the luminance of $CsPbI_3$ and $CsPbI_{2.85}Br_{0.15}$ NCs-based LED devices only reached 610 cd/m^2 and 1601 cd/m^2, respectively.

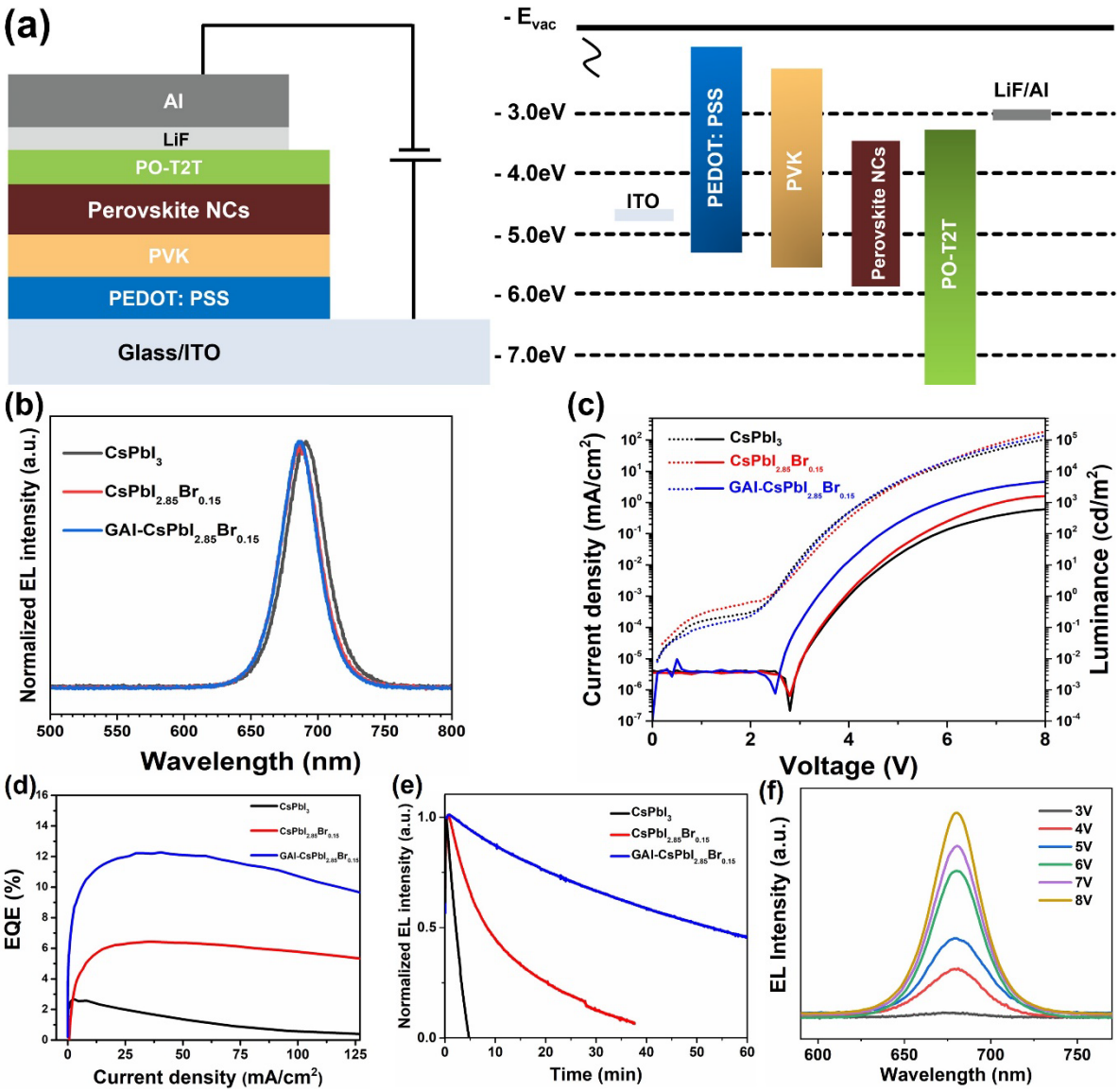

Figure 4. Red PeLED device fabrication and performance evaluation. (**a)** Illustration and band structure of $CsPbI_3$ NCs LEDs device configuration (detailed in Figure S11). (**b)** Electroluminescence of the LEDs device made from pristine $CsPbI_{2.85}Br_{0.15}$ and GAI-$CsPbI_{2.85}Br_{0.15}$ NCs, respectively (100mA cm^{-2}, ~ 8V). Operational characteristics for PeLEDs based on pristine, $CsPbI_{2.85}Br_{0.15}$ and GAI-$CsPbI_{2.85}Br_{0.15}$ NCs: (**c)** Current density–voltage curves (dotted line) and luminance–voltage curves (solid line). (**d)** EQE–current density curves. (**e)** EL spectral stability under continuous operation at a constant current density of 20 mA cm^{-2} (The EQE of the three samples at 20 mA cm^{-2} are 12%, 6% and 2% respectively). (**f)** EL spectral stability of GAI-$CsPbI_{2.85}Br_{0.15}$ NCs-based PeLED under different bias voltage.

Furthermore, the LED devices with GAI-$CsPbI_{2.85}Br_{0.15}$ NCs showed a high EQE of 12.35%, which is remarkably higher than the device based on pristine $CsPbI_3$ NCs (2.28%) and $CsPbI_{2.85}Br_{0.15}$ NCs (6.16%) (Figure 4d). Such significantly improved GAI-$CsPbI_{2.85}Br_{0.15}$ NCs LED performance should be attributed to the improved building blocks, resulting in excellent emission properties (high luminescence and high current density) due to improved charge transport. To better understand the role of phenacyl bromide post-treatment and MeOAC anti-solvent purification in photonic devices, we also fabricated LED devices based on i) typical Br doping with $PbBr_2$, $PbBr_2$-$CsPbI_{2.85}Br_{0.15}$, and ii) $CsPbI_3$ NCs secondary purification by MeOAC. It can be observed that the excess MeOAC washing significantly deteriorated the performance of the NCs as evidenced by a reduced

EQE from 2.3% to 1.7% and lower current density (Figure S8). The maximum EQE of the $PbBr_2$-$CsPbI_{2.85}Br_{0.15}$ device is 5.7%. Still, the radiance luminance is relatively lower than the phenacyl bromide post-treated $CsPbI_{2.85}Br_{0.15}$ device, indicating more nonradiative combination losses existed inside the typical $PbBr_2$-doped NC film (Figure S8). From the top-view SEM images of the $CsPbI_3$ NCs films (Figure S9), all three studied cases exhibit homogeneous films with good coverage, avoiding the possible current leakage during device operation.

To examine the operational stability in our optimized perovskite films, we measured the EL spectra of devices using GAI-$CsPbI_{2.85}Br_{0.15}$ emitting layers either under constant current density (20 mA/cm^2) (Figure 4e) and luminance spectra under increasing voltage bias (Figure 4f). Previous works shows that Br-rich perovskites exhibit irreversible phase segregation, prominently induced by halide ion migration under applied voltage bias[59]. In our case, no changes in EL spectra were observed under different biases, confirming no phase segregation in the perovskite layer composition. The device was then operated at a constant current density (20 mA/cm^2), and the luminance of the device was recorded. Benefiting from the enhanced phase stability and the suppressed defects, the LED-based on GAI-$CsPbI_{2.85}Br_{0.15}$ NCs films showed optimized operational stability with an operating half-lifetime T_{50} of 50 mins. In contrast, the LED-based on $CsPbI_{2.85}Br_{0.15}$ NCs exhibited a T_{50} of 20 min, and the EL emission intensity of the LED with pristine $CsPbI_3$ NCs dropped rapidly to half of the initial value in 7 min. The performances of recently developed $CsPbI_{3-x}Br_x$ NC-based LEDs employing different surface treatment methods are summarized in comparison with the devices developed in our work, in Table S2. To better compare with the device stability in the literature, we also measured the operational stability of our optimized device at different constant current densities (Figure S12). The optimized device operational stability exceeds 7 hrs when the device is operated at 5 mA cm^{-2} current density. Compared to the literature, our LED devices exhibit excellent luminance and operational stability simultaneously. All results above clearly demonstrate the beneficial effect of the phenacyl bromide doping and GAI passivation method on the device performance and stability of $CsPbI_{3-x}Br_x$ NCs-based LEDs.

3. Conclusions

In conclusion, our work demonstrates guanidinium iodide post-treatment as a facile and feasible passivation strategy for all-inorganic perovskite NCs, resulting in outstanding optoelectronic properties. Due to the excellent surface passivation property of the guanidinium cation with multiple amino groups, the surface treatment led to the enhanced luminescence and stability of the NCs. Outstanding properties of the passivated $CsPbI_{3-x}Br_x$ NCs are identified, including increased PL lifetimes and reduced PL blinking probability. These stable NCs were used to produce bright-red LEDs that exhibit narrow electroluminescence at 685 nm, a lower turn-on voltage, and reach a maximum luminance of 4624 cd/m^2 at 8 V. The devices exhibit spectrally stable electroluminescence at 5.5 V and achieve an excellent EQE of 12.35%. The operational half-life improved by a 7-folds relative to control devices, reaching T_{50} of 50 min at 20 mA/cm^2. Our work uncovers a new approach for the stabilization of perovskite NCs for higher-performance photonic devices by using amino-rich ligands.

4. Experimental Section

4.1. Materials

Lead iodide (PbI_2, super dry, 99%), cesium carbonate (Cs_2CO_3, 99.95%), oleic acid (OA, ≥90%), 1-octadecene (ODE, 90%), oleylamine (OAm, 80-90%), methyl acetate (MeOAC, 99.9%), hexane, tetrahydrofuran (THF, 99.99%), toluene (anhydrous, 99.8%), *N*, *N*-dimethylformamide (DMF, anhydrous, 99.8%) and lithium fluoride (LiF) were obtained from Sigma-Aldrich. Guanidine iodide (GAI, 99%), phenacyl bromide (99%) were purchased from Alfa Aesar. Poly(3,4-ethylene dioxythiophene)

(PEDOT:PSS) was obtained from Heraeus, Poly[*N,N'*-bis (4-butyl phenyl)-*N,N'*-bis(phenyl)-benzidine] (PolyTPD), (Polyvinylcarbazole) PVK, and 2,4,6-Tris[3-(diphenylphosphinyl)phenyl]-1,3,5-triazine (PO-T2T) were purchased from American Dye Source and Lumtec, respectively. Moisture sensitive compounds were stored in glovebox before use. All the commercial materials were used as received without further purification.

4.2. Synthesis of Perovskite NCs

The synthesis protocols were carried out by a typical hot-injection method[38, 60-61] with some modifications. First, Cs-oleate was prepared by adding 400 mg Cs_2CO_3 and 15 mL ODE into a 100 mL three-neck round bottom flask. The flask was then degassed under vacuum at 120 °C for 30 min. Subsequently, 1.725 mL OA was added to the solution, and the system was heated under a vacuum and stirred until the Cs_2CO_3 was dissolved entirely, resulting in a clear solution. Afterwards, the mixture was heated to 150 °C under nitrogen and degassed for another 30 min. The Cs-oleate solution was then stored under nitrogen for further use.

For pure $CsPbI_3$ NCs synthesis, 334 mg PbI_2, 10 mL ODE, 2 mL OA, and 2 mL OAm were loaded in a three-neck round bottom flask. The flask was degassed and dried under vacuum for 1 hr at 120 °C with stirring. After PbI_2 was dissolved entirely, the system was transferred to N_2 gas and further stirred for 20 mins. Afterwards, the temperature was raised; once the temperature reached to 170 °C, 1.6 mL of as-prepared Cs-oleate (preheated at 100 °C) was quickly injected into the solution. About 5 s later, the reaction was quenched by quickly immersing the flask in an ice-water bucket. After the flask was cooled down to room temperature, the solution was equally transferred to two 50 mL centrifuge vials, and 10 mL of MeOAC was added to precipitate and purify the NCs. The NCs were then collected by centrifugation at 8700 rpm for 10 min. After that, the supernatant is discarded, and the collected NCs are dispersed in 2 mL of octane. The collected NCs are stored at 4 °C for 48 h. After this stage, unreacted precursor agents and any excess of surface ligands would precipitate the final supernatant was collected for further measurement and applications. $CsPb(I/Br)_3$ NCs with different Br doping percentages were obtained by changing the amount of phenacyl bromide (14.9 mg, 29.8mg, and 59.7 mg, respectively representing 5%, 10%, and 20% Br-doped samples). Since we introduced phenacyl bromide as the source of bromine, the PbI_2 dissolution temperature was increased to 220 °C, 2 ml OAm was injected, and after 20 minutes of reaction, the system temperature was reduced to 150 °C until the solution became transparent. Then the Cs-oleate precursor was rapidly injected while increasing the solution temperature to 170 °C and ice bathing after 5 s reaction to synthesize high-quality and stable $CsPbI_{3-x}Br_x$ NCs. Purification and storage procedures are similar to pure $CsPbI_3$.

4.3. Surface treatment

The as-synthesized NCs were diluted in octane to a specific concentration (20 mg/mL). 74.8 mg GAI was dissolved in 2 mL THF to make the passivation solution. Then, different quantities of the GAI solution were added to 2 mL of the $CsPbI_3$ NCs solution and stirred for 3 min. After that, the NCs were recollected by centrifuging at 8700 rpm for 5 min. The supernatant was discarded, and the precipitate was collected and dispersed into 2 ml octane for further use.

4.4. Light-Emitting Diode Fabrication

LED devices using pristine or GAI-treated $CsPbI_{3-x}Br_x$ NCs as light-emitting layers were fabricated using pre-patterned ITO (Colorado Concept Coatings) deposited glass substrates. Before fabrication, the ITO substrates were ultra-sonicated in soap water, Milli-Q water, acetone, and isopropanol consecutively, for 10 min each. The ITO substrates were blow-dried with compressed N_2 gas and UV-Ozone treated for 15 min before spin-coating other layers. A PEDOT-PVK tightly bound coating was used as a hole injection layer in all LED devices in the experiments. PEDOT was filtered by a 0.45 µm PVDF filter and then spin-coated on precleaned ITO at 5000 rpm for 60 s using a spincoater (Laurell Technologies). The spin-coated PEDOT ITO

substrates were placed on a heating plate and then annealed at 120 °C for 20 min. After annealing, the substrates were transferred to a glove box system with low moisture and oxygen (sub-ppm) levels. PVK was spin-coated at 4000 rpm for 60 s, followed by thermal annealing at 150 °C for 20 min. After that, the homogenous perovskite emitting layer was deposited by optimized spin-coating conditions (4000 rpm for 40s) in the N_2-filled glove box. After emitting layer deposition, samples were transferred to another glove box. Then, PO-T2T, LiF, and Al layers were thermally evaporated on top of the perovskite films sequentially, with thicknesses of 40, 1.2, and 120 nm, respectively, at pressures of ~ 10^{-7} mbar. The device area was 0.125 cm^2 with dimensions of 2.5 × 5 mm.

4.5. Characterizations

The ultraviolet-visible (UV-vis) diffuse reflectance spectra were measured using a Lambda 950 UV-vis spectrophotometer. PL measurements were performed on an Edinburgh FLS980 using a He-Cd laser with a 470 nm excitation wavelength at room temperature. Lifetime spectra were measured using Leica TCS SP8 X 'FLIM' measurements with a 470 nm laser at a 10 MHz repetition rate.

Bright-field Transmission Electron Microscopy (BF-TEM) analyses were performed by means of a JEM-1400Plus microscope (JEOL) equipped with LaB6 thermionic gun, operated at 120 kV. Specimens were prepared drop-casting 2 µL of NCs hexane suspension on an ultrathin carbon coated copper grid. Size distribution of NCs was obtained from TEM images measuring the edge size of approximately 100 NCs using Gatan Digital Micrograph software. Selected Area Electron Diffraction (SAED) patterns were processed thanks to Scikit-ued Python package. The film XRD pattern was obtained on a Bruker AXS D8 diffractometer using Cu Kα radiation. Stability measurements of the NCs structure were carried out by measuring the XRD pattern at different time intervals after the film was stored in ambient conditions. The Fourier transform infrared (FTIR) spectra of the NC thin films were recorded using an Agilent Technologies FTIR spectrometer. The NCs were spin-coated on a glass substrate and FTIR spectra were recorded after the solvent was evaporated.

The response of the photodiode was calibrated applying the integrating sphere by Thorlabs. In addition, the J-V and L-V characteristics were measured by an Agilent 4156C Semiconductor Parameter Analyzer, which also records the corresponding photodiode current simultaneously.

The single-particle PL intensity time traces were recorded by an inverted wide-field fluorescence microscope (Olympus IX83) equipped with 60 x objective lens and 2.5 projection lens. On a glass coverslip (24 × 24 mm, Thermo Scientific), a very dilute solution of $CsPbI_{3-x}Br_x$ NCs was drop-casted, the sample was excited with the laser, and the emission signals were recorded. The emission light was collected by an EM-CCD camera (Image-EM X2, Hamamatsu). All data were recorded over 4000 frames with an exposure time of 30 ms (total duration of 120 s). A 561 nm continuous wave laser and 665 nm long-pass emission filter were used for the experiment.

Acknowledgments

B.P. acknowledges support from the Research Foundation-Flanders through a postdoctoral fellowship (FWO Grant No. 1275521N). J.H., E.D., and M.R. acknowledge financial support from the Research Foundation- (FWO) through research projects (FWO Grant No's G098319, , S002019N "PROCEED", S004322N "GIGAPIXEL"), from the Flemish government through long-term structural funding Methusalem (CASAS2, Meth/15/04), through iBOF funding (PERsist: iBOF-21-085) and from the KU Leuven Research Fund (grants C14/19/079 and STG/21/010). Y. Z. acknowledges support from the China Scholarship Council (No. 201908440479). K.E. acknowledges funding from the European Research Council under the European Horizon 2020 Programme/ERC grant agreement no. 835133 (ULTRA-LUX)

References

(1) Hairen Tan, A. J., Oleksandr Voznyy, Xinzheng Lan, F. Pelayo García de Arquer, et al. Efficient and stable solution-processed planar perovskite solar cells via contact passivation. *Science* **2017,** *355* (6326), 722-726, DOI: 10.1126/science.aai9081.
(2) Liang, J.; Wang, C.; Wang, Y.; Xu, Z.; Lu, Z.; Ma, Y.; Zhu, H.; Hu, Y.; Xiao, C.; Yi, X.; Zhu, G.; Lv, H.; Ma, L.; Chen, T.; Tie, Z.; Jin, Z.; Liu, J. All-Inorganic Perovskite Solar Cells. *J. Am. Chem. Soc.* **2016,** *138* (49), 15829-15832, DOI: 10.1021/jacs.6b10227.
(3) Voznyy, O. Black and Stable: A Path to All-Inorganic Halide Perovskite Solar Cells. *Joule* **2018,** *2* (7), 1215-1216, DOI: 10.1016/j.joule.2018.07.001.
(4) Zhou, Y.; Chen, J.; Bakr, O. M.; Mohammed, O. F. Metal Halide Perovskites for X-ray Imaging Scintillators and Detectors. *ACS Energy Lett.* **2021,** *6* (2), 739-768, DOI: 10.1021/acsenergylett.0c02430.
(5) Clinckemalie, L.; Valli, D.; Roeffaers, M. B. J.; Hofkens, J.; Pradhan, B.; Debroye, E. Challenges and Opportunities for CsPbBr3 Perovskites in Low- and High-Energy Radiation Detection. *ACS Energy Lett.* **2021,** *6* (4), 1290-1314, DOI: 10.1021/acsenergylett.1c00007.
(6) Dey, A.; Ye, J.; De, A.; Debroye, E.; Ha, S. K.; Bladt, E.; Kshirsagar, A. S.; Wang, Z.; Yin, J.; Wang, Y.; Quan, L. N.; Yan, F.; Gao, M.; Li, X.; Shamsi, J.; Debnath, T.; Cao, M.; Scheel, M. A.; Kumar, S.; Steele, J. A.; Gerhard, M.; Chouhan, L.; Xu, K.; Wu, X. G.; Li, Y.; Zhang, Y.; Dutta, A.; Han, C.; Vincon, I.; Rogach, A. L.; Nag, A.; Samanta, A.; Korgel, B. A.; Shih, C. J.; Gamelin, D. R.; Son, D. H.; Zeng, H.; Zhong, H.; Sun, H.; Demir, H. V.; Scheblykin, I. G.; Mora-Sero, I.; Stolarczyk, J. K.; Zhang, J. Z.; Feldmann, J.; Hofkens, J.; Luther, J. M.; Perez-Prieto, J.; Li, L.; Manna, L.; Bodnarchuk, M. I.; Kovalenko, M. V.; Roeffaers, M. B. J.; Pradhan, N.; Mohammed, O. F.; Bakr, O. M.; Yang, P.; Muller-Buschbaum, P.; Kamat, P. V.; Bao, Q.; Zhang, Q.; Krahne, R.; Galian, R. E.; Stranks, S. D.; Bals, S.; Biju, V.; Tisdale, W. A.; Yan, Y.; Hoye, R. L. Z.; Polavarapu, L. State of the Art and Prospects for Halide Perovskite Nanocrystals. *ACS Nano* **2021,** *15* (7), 10775-10981, DOI: 10.1021/acsnano.0c08903.
(7) Wang, Z.; Shen, X.; Tang, C.; Li, X.; Hu, J.; Zhu, J.; Yu, W. W.; Song, H.; Bai, X. Efficient and Stable CF3PEAI-Passivated CsPbI3 QDs toward Red LEDs. *ACS Appl. Mater. Interfaces* **2022,** *14* (6), 8235-8242, DOI: 10.1021/acsami.1c19685.
(8) Zhang, L.; Yang, X.; Jiang, Q.; Wang, P.; Yin, Z.; Zhang, X.; Tan, H.; Yang, Y. M.; Wei, M.; Sutherland, B. R.; Sargent, E. H.; You, J. Ultra-bright and highly efficient inorganic based perovskite light-emitting diodes. *Nat. Commun.* **2017,** *8*, 15640, DOI: 10.1038/ncomms15640.
(9) Jin, H.; Debroye, E.; Keshavarz, M.; Scheblykin, I. G.; Roeffaers, M. B. J.; Hofkens, J.; Steele, J. A. It's a trap! On the nature of localised states and charge trapping in lead halide perovskites. *Materials Horizons* **2020,** *7* (2), 397-410, DOI: 10.1039/c9mh00500e.
(10) Ban, M.; Zou, Y.; Rivett, J. P. H.; Yang, Y.; Thomas, T. H.; Tan, Y.; Song, T.; Gao, X.; Credgington, D.; Deschler, F.; Sirringhaus, H.; Sun, B. Solution-processed perovskite light emitting diodes with efficiency exceeding 15% through additive-controlled nanostructure tailoring. *Nat. Commun.* **2018,** *9* (1), 3892, DOI: 10.1038/s41467-018-06425-5.
(11) Boles, M. A.; Ling, D.; Hyeon, T.; Talapin, D. V. Erratum: The surface science of nanocrystals. *Nat Mater* **2016,** *15* (3), 364, DOI: 10.1038/nmat4578.
(12) Hoang, M. T.; Pannu, A. S.; Tang, C.; Yang, Y.; Pham, N. D.; Gui, K.; Wang, X.; Yambem, S.; Sonar, P.; Du, A.; Wang, H. Potassium Doping to Enhance Green Photoemission of Light‐Emitting Diodes Based on $CsPbBr_3$ Perovskite Nanocrystals. *Adv. Opt. Mater.* **2020,** *8* (18), 2000742, DOI: 10.1002/adom.202000742.
(13) Protesescu, L.; Yakunin, S.; Bodnarchuk, M. I.; Krieg, F.; Caputo, R.; Hendon, C. H.; Yang, R. X.; Walsh, A.; Kovalenko, M. V. Nanocrystals of Cesium Lead Halide Perovskites (CsPbX(3), X = Cl, Br, and I): Novel Optoelectronic Materials Showing Bright Emission with Wide Color Gamut. *Nano Lett* **2015,** *15* (6), 3692-6, DOI: 10.1021/nl5048779.
(14) Yang, J. N.; Chen, T.; Ge, J.; Wang, J. J.; Yin, Y. C.; Lan, Y. F.; Ru, X. C.; Ma, Z. Y.; Zhang, Q.; Yao, H. B. High Color Purity and Efficient Green Light-Emitting Diode Using Perovskite Nanocrystals with the Size Overly Exceeding Bohr Exciton Diameter. *J. Am. Chem. Soc.* **2021,** *143* (47), 19928-19937, DOI: 10.1021/jacs.1c09948.
(15) Nakanotani, H.; Higuchi, T.; Furukawa, T.; Masui, K.; Morimoto, K.; Numata, M.; Tanaka, H.; Sagara, Y.; Yasuda, T.; Adachi, C. High-efficiency organic light-emitting diodes with fluorescent emitters. *Nat. Commun.* **2014,** *5*, 4016, DOI: 10.1038/ncomms5016.
(16) Kim, Y.-H.; Kim, S.; Kakekhani, A.; Park, J.; Park, J.; Lee, Y.-H.; Xu, H.; Nagane, S.; Wexler, R. B.; Kim, D.-H.; Jo, S. H.; Martínez-Sarti, L.; Tan, P.; Sadhanala, A.; Park, G.-S.; Kim, Y.-W.; Hu, B.; Bolink, H. J.; Yoo, S.; Friend, R. H.; Rappe, A. M.; Lee, T.-W. Comprehensive defect suppression in perovskite nanocrystals for high-efficiency light-emitting diodes. *Nature Photon.* **2021**, DOI: 10.1038/s41566-020-00732-4.
(17) Wang, Y. K.; Yuan, F.; Dong, Y.; Li, J. Y.; Johnston, A.; Chen, B.; Saidaminov, M. I.; Zhou, C.; Zheng, X.; Hou, Y.; Bertens, K.; Ebe, H.; Ma, D.; Deng, Z.; Yuan, S.; Chen, R.; Sagar, L. K.; Liu, J.; Fan, J.; Li, P.; Li, X.; Gao, Y.; Fung, M. K.; Lu, Z. H.; Bakr, O. M.; Liao, L. S.; Sargent, E. H. All-Inorganic Quantum-Dot LEDs Based on a Phase-Stabilized alpha-CsPbI3 Perovskite. *Angew. Chem. Int. Ed. Engl.* **2021,** *60* (29), 16164-16170, DOI: 10.1002/anie.202104812.
(18) Miao, Y.; Liu, X.; Chen, Y.; Zhang, T.; Wang, T.; Zhao, Y. Deep-Red Perovskite Light-Emitting Diodes Based on One-Step-Formed gamma-CsPbI3 Cuboid Crystallites. *Adv. Mater.* **2021,** *33* (51), e2105699, DOI: 10.1002/adma.202105699.
(19) Lan, Y. F.; Yao, J. S.; Yang, J. N.; Song, Y. H.; Ru, X. C.; Zhang, Q.; Feng, L. Z.; Chen, T.; Song, K. H.; Yao, H. B. Spectrally Stable and Efficient Pure Red CsPbI3 Quantum Dot Light-Emitting Diodes Enabled by Sequential Ligand Post-Treatment Strategy. *Nano Lett* **2021,** *21* (20), 8756-8763, DOI: 10.1021/acs.nanolett.1c03011.

(20) Yan, F.; Tan, S. T.; Li, X.; Demir, H. V. Light Generation in Lead Halide Perovskite Nanocrystals: LEDs, Color Converters, Lasers, and Other Applications. *Small* **2019,** *15* (47), e1902079, DOI: 10.1002/smll.201902079.
(21) Abhishek Swarnkar, A. R. M., Erin M. Sanehira, Boris D. Chernomordik, David T. Moore, Jeffrey A. Christians, Tamoghna Chakrabarti, Joseph M. Luther. Quantum dot–induced phase stabilization of α-CsPbI3 perovskite for high-efficiency photovoltaics. *Science* **2016,** *354* (6308), 92-95, DOI: 10.1126/science.aag270.
(22) Han, B.; Cai, B.; Shan, Q.; Song, J.; Li, J.; Zhang, F.; Chen, J.; Fang, T.; Ji, Q.; Xu, X.; Zeng, H. Stable, Efficient Red Perovskite Light-Emitting Diodes by (α, δ)-$CsPbI_3$ Phase Engineering. *Adv. Funct. Mater.* **2018,** *28* (47), 1804285, DOI: 10.1002/adfm.201804285.
(23) Mir, W. J.; Alamoudi, A.; Yin, J.; Yorov, K. E.; Maity, P.; Naphade, R.; Shao, B.; Wang, J.; Lintangpradipto, M. N.; Nematulloev, S.; Emwas, A. H.; Genovese, A.; Mohammed, O. F.; Bakr, O. M. Lecithin Capping Ligands Enable Ultrastable Perovskite-Phase CsPbI3 Quantum Dots for Rec. 2020 Bright-Red Light-Emitting Diodes. *J. Am. Chem. Soc.* **2022,** *144* (29), 13302-13310, DOI: 10.1021/jacs.2c04637.
(24) Julian A. Steele, H. J., Iurii Dovgaliuk et al. Thermal unequilibrium of strained black $CsPbI_3$ thin films. *Science* **2019,** *365* (6454), 679–684, DOI: 10.1126/science.aax3878.
(25) Wang, Y.; Zhang, T.; Kan, M.; Zhao, Y. Bifunctional Stabilization of All-Inorganic alpha-CsPbI3 Perovskite for 17% Efficiency Photovoltaics. *J. Am. Chem. Soc.* **2018,** *140* (39), 12345-12348, DOI: 10.1021/jacs.8b07927.
(26) Sun, K.; Gao, C.; Yang, C.; Liu, H.; Hu, Z.; Zhang, J.; Zhu, Y. Direct formed tri-iodide ions stabilizing colloidal precursor solution and promoting the reproducibility of perovskite solar cells by solution process. *Electrochim. Acta* **2019,** *311*, 132-140, DOI: 10.1016/j.electacta.2019.04.123.
(27) De Roo, J.; Ibanez, M.; Geiregat, P.; Nedelcu, G.; Walravens, W.; Maes, J.; Martins, J. C.; Van Driessche, I.; Kovalenko, M. V.; Hens, Z. Highly Dynamic Ligand Binding and Light Absorption Coefficient of Cesium Lead Bromide Perovskite Nanocrystals. *ACS Nano* **2016,** *10* (2), 2071-81, DOI: 10.1021/acsnano.5b06295.
(28) Mir, W. J.; Swarnkar, A.; Nag, A. Postsynthesis Mn-doping in CsPbI3 nanocrystals to stabilize the black perovskite phase. *Nanoscale* **2019,** *11* (10), 4278-4286, DOI: 10.1039/c9nr00248k.
(29) Yang, J. N.; Song, Y.; Yao, J. S.; Wang, K. H.; Wang, J. J.; Zhu, B. S.; Yao, M. M.; Rahman, S. U.; Lan, Y. F.; Fan, F. J.; Yao, H. B. Potassium Bromide Surface Passivation on CsPbI3-xBrx Nanocrystals for Efficient and Stable Pure Red Perovskite Light-Emitting Diodes. *J. Am. Chem. Soc.* **2020,** *142* (6), 2956-2967, DOI: 10.1021/jacs.9b11719.
(30) Tseng, Z. L.; Chen, L. C.; Chao, L. W.; Tsai, M. J.; Luo, D.; Al Amin, N. R.; Liu, S. W.; Wong, K. T. Aggregation Control, Surface Passivation, and Optimization of Device Structure toward Near-Infrared Perovskite Quantum-Dot Light-Emitting Diodes with an EQE up to 15.4. *Adv. Mater.* **2022,** *34* (18), e2109785, DOI: 10.1002/adma.202109785.
(31) Liang, A.; Wang, K.; Gao, Y.; Finkenauer, B. P.; Zhu, C.; Jin, L.; Huang, L.; Dou, L. Highly Efficient Halide Perovskite Light-Emitting Diodes via Molecular Passivation. *Angew. Chem. Int. Ed. Engl.* **2021,** *60* (15), 8337-8343, DOI: 10.1002/anie.202100243.
(32) Bhatia, H.; Steele, J. A.; Martin, C.; Keshavarz, M.; Solis-Fernandez, G.; Yuan, H.; Fleury, G.; Huang, H.; Dovgaliuk, I.; Chernyshov, D.; Hendrix, J.; Roeffaers, M. B. J.; Hofkens, J.; Debroye, E. Single-Step Synthesis of Dual Phase Bright Blue-Green Emitting Lead Halide Perovskite Nanocrystal Thin Films. *Chem. Mater.* **2019,** *31* (17), 6824-6832, DOI: 10.1021/acs.chemmater.9b01277.
(33) Soe, C. M. M.; Stoumpos, C. C.; Kepenekian, M.; Traore, B.; Tsai, H.; Nie, W.; Wang, B.; Katan, C.; Seshadri, R.; Mohite, A. D.; Even, J.; Marks, T. J.; Kanatzidis, M. G. New Type of 2D Perovskites with Alternating Cations in the Interlayer Space, (C(NH2)3)(CH3NH3)nPbnI3n+1: Structure, Properties, and Photovoltaic Performance. *J. Am. Chem. Soc.* **2017,** *139* (45), 16297-16309, DOI: 10.1021/jacs.7b09096.
(34) Zhang, Y.; Keshavarz, M.; Debroye, E.; Fron, E.; Rodríguez González, M. C.; Naumenko, D.; Amenitsch, H.; Van de Vondel, J.; De Feyter, S.; Heremans, P.; Roeffaers, M. B. J.; Qiu, W.; Pradhan, B.; Hofkens, J. Two-dimensional perovskites with alternating cations in the interlayer space for stable light-emitting diodes. *Nanophotonics* **2021,** *10* (8), 2145-2156, DOI: 10.1515/nanoph-2021-0037.
(35) Jiang, M.; Hu, Z.; Ono, L. K.; Qi, Y. CsPbBrxI3-x thin films with multiple ammonium ligands for low turn-on pure-red perovskite light-emitting diodes. *Nano Res.* **2020,** *14* (1), 191-197, DOI: 10.1007/s12274-020-3065-5.
(36) Liu, J.; Leng, J.; Wu, K.; Zhang, J.; Jin, S. Observation of Internal Photoinduced Electron and Hole Separation in Hybrid Two-Dimentional Perovskite Films. *J. Am. Chem. Soc.* **2017,** *139* (4), 1432-1435, DOI: 10.1021/jacs.6b12581.
(37) ten Brinck, S.; Infante, I. Surface Termination, Morphology, and Bright Photoluminescence of Cesium Lead Halide Perovskite Nanocrystals. *ACS Energy Lett.* **2016,** *1* (6), 1266-1272, DOI: 10.1021/acsenergylett.6b00595.
(38) Pradhan, B.; Mushtaq, A.; Roy, D.; Sain, S.; Das, B.; Ghorai, U. K.; Pal, S. K.; Acharya, S. Postsynthesis Spontaneous Coalescence of Mixed-Halide Perovskite Nanocubes into Phase-Stable Single-Crystalline Uniform Luminescent Nanowires. *J Phys. Chem. Lett.* **2019,** *10* (8), 1805-1812, DOI: 10.1021/acs.jpclett.9b00832.
(39) Lu, M.; Guo, J.; Sun, S.; Lu, P.; Wu, J.; Wang, Y.; Kershaw, S. V.; Yu, W. W.; Rogach, A. L.; Zhang, Y. Bright CsPbI3 Perovskite Quantum Dot Light-Emitting Diodes with Top-Emitting Structure and a Low Efficiency Roll-Off Realized by Applying Zirconium Acetylacetonate Surface Modification. *Nano Lett* **2020,** *20* (4), 2829-2836, DOI: 10.1021/acs.nanolett.0c00545.
(40) Sutton, R. J.; Filip, M. R.; Haghighirad, A. A.; Sakai, N.; Wenger, B.; Giustino, F.; Snaith, H. J. Cubic or Orthorhombic? Revealing the Crystal Structure of Metastable Black-Phase CsPbI3 by Theory and Experiment. *ACS Energy Lett.* **2018,** *3* (8), 1787-1794, DOI: 10.1021/acsenergylett.8b00672.

(41) Ling, X.; Yuan, J.; Zhang, X.; Qian, Y.; Zakeeruddin, S. M.; Larson, B. W.; Zhao, Q.; Shi, J.; Yang, J.; Ji, K.; Zhang, Y.; Wang, Y.; Zhang, C.; Duhm, S.; Luther, J. M.; Gratzel, M.; Ma, W. Guanidinium-Assisted Surface Matrix Engineering for Highly Efficient Perovskite Quantum Dot Photovoltaics. *Adv. Mater.* **2020,** *32* (26), e2001906, DOI: 10.1002/adma.202001906.
(42) Shin, Y. S.; Yoon, Y. J.; Lee, K. T.; Lee, W.; Kim, H. S.; Kim, J. W.; Jang, H.; Kim, M.; Kim, D. S.; Kim, G. H.; Kim, J. Y. High-Performance Perovskite Light-Emitting Diodes with Surface Passivation of CsPbBr(x)I(3-x) Nanocrystals via Antisolvent-Triggered Ion-Exchange. *ACS Appl. Mater. Interfaces* **2020,** *12* (28), 31582-31590, DOI: 10.1021/acsami.0c06213.
(43) Ma, Q.; Huang, S.; Wen, X.; Green, M. A.; Ho-Baillie, A. W. Y. Hole Transport Layer Free Inorganic CsPbIBr2 Perovskite Solar Cell by Dual Source Thermal Evaporation. *Adv. Energy Mater.* **2016,** *6* (7), 1502202, DOI: 10.1002/aenm.201502202.
(44) Yuan, L.; Sun, X.; Zhang, X.; Li, F.; Liu, Y.; Gao, Y.; Qian, H.; Liu, Z.; Ma, W. Targeted Design of Surface Configuration on CsPbI3 Perovskite Nanocrystals for High-Efficiency Photovoltaics. *ACS Energy Lett.* **2022**, 241-249, DOI: 10.1021/acsenergylett.2c02453.
(45) Shi, Z.-E.; Long, J.-Y.; Li, C.-W.; Hsieh, S.-Y.; Hsiao, Y.-S.; Chen, C.-P.; Yu, Y.-H. A multifunctional ligand for defect passivation of perovskite film realizes air-stable perovskite solar cells with efficiencies exceeding 20%. *Sustain. Energy Fuels* **2022,** *6* (8), 1950-1958, DOI: 10.1039/d1se01892b.
(46) Yang, X.; Zhang, X.; Deng, J.; Chu, Z.; Jiang, Q.; Meng, J.; Wang, P.; Zhang, L.; Yin, Z.; You, J. Efficient green light-emitting diodes based on quasi-two-dimensional composition and phase engineered perovskite with surface passivation. *Nat. Commun.* **2018,** *9* (1), 570, DOI: 10.1038/s41467-018-02978-7.
(47) Chen, W.; Pham, N. D.; Wang, H.; Jia, B.; Wen, X. Spectroscopic Insight into Efficient and Stable Hole Transfer at the Perovskite/Spiro-OMeTAD Interface with Alternative Additives. *ACS Appl. Mater. Interfaces* **2021,** *13* (4), 5752-5761, DOI: 10.1021/acsami.0c19111.
(48) De Marco, N.; Zhou, H.; Chen, Q.; Sun, P.; Liu, Z.; Meng, L.; Yao, E. P.; Liu, Y.; Schiffer, A.; Yang, Y. Guanidinium: A Route to Enhanced Carrier Lifetime and Open-Circuit Voltage in Hybrid Perovskite Solar Cells. *Nano Lett.* **2016,** *16* (2), 1009-16, DOI: 10.1021/acs.nanolett.5b04060.
(49) Galland, C.; Ghosh, Y.; Steinbruck, A.; Sykora, M.; Hollingsworth, J. A.; Klimov, V. I.; Htoon, H. Two types of luminescence blinking revealed by spectroelectrochemistry of single quantum dots. *Nature* **2011,** *479* (7372), 203-7, DOI: 10.1038/nature10569.
(50) Young-Shin Park; Shaojun Guo; Nikolay S. Makarov; Klimov., V. I. Room Temperature Single-Photon Emission from Individual Perovskite Quantum Dots. *ACS Nano* **2015,** *9* (10), 10386-10393, DOI: 10.1021/acsnano.5b04584.
(51) Eremchev, I. Y.; Tarasevich, A. O.; Li, J.; Naumov, A. V.; Scheblykin, I. G. Lack of Photon Antibunching Supports Supertrap Model of Photoluminescence Blinking in Perovskite Sub‐Micrometer Crystals. *Adv. Opt. Mater.* **2020,** *9* (3), 2001596, DOI: 10.1002/adom.202001596.
(52) Chouhan, L.; Ito, S.; Thomas, E. M.; Takano, Y.; Ghimire, S.; Miyasaka, H.; Biju, V. Real-Time Blinking Suppression of Perovskite Quantum Dots by Halide Vacancy Filling. *ACS Nano* **2021,** *15* (2), 2831-2838, DOI: 10.1021/acsnano.0c08802.
(53) Jin, H.; Steele, J. A.; Cheng, R.; Parveen, N.; Roeffaers, M. B. J.; Hofkens, J.; Debroye, E. Experimental Evidence of Chloride‐Induced Trap Passivation in Lead Halide Perovskites through Single Particle Blinking Studies. *Adv. Opt. Mater.* **2021,** *9* (23), 2002240, DOI: 10.1002/adom.202002240.
(54) Smock, S. R.; Chen, Y.; Rossini, A. J.; Brutchey, R. L. The Surface Chemistry and Structure of Colloidal Lead Halide Perovskite Nanocrystals. *Acc. Chem. Res.* **2021,** *54* (3), 707-718, DOI: 10.1021/acs.accounts.0c00741.
(55) Li, Y.; Hou, X.; Dai, X.; Yao, Z.; Lv, L.; Jin, Y.; Peng, X. Stoichiometry-Controlled InP-Based Quantum Dots: Synthesis, Photoluminescence, and Electroluminescence. *J. Am. Chem. Soc.* **2019,** *141* (16), 6448-6452, DOI: 10.1021/jacs.8b12908.
(56) Gerhard, M.; Louis, B.; Frantsuzov, P. A.; Li, J.; Kiligaridis, A.; Hofkens, J.; Scheblykin, I. G. Heterogeneities and Emissive Defects in MAPbI3 Perovskite Revealed by Spectrally Resolved Luminescence Blinking. *Adv. Opt. Mater.* **2021,** *9* (18), 2001380, DOI: 10.1002/adom.202001380.
(57) Yuan, G.; Ritchie, C.; Ritter, M.; Murphy, S.; Gómez, D. E.; Mulvaney, P. The Degradation and Blinking of Single CsPbI3 Perovskite Quantum Dots. *J. Phys. Chem. C* **2017,** *122* (25), 13407-13415, DOI: 10.1021/acs.jpcc.7b11168.
(58) Qiu, W.; Xiao, Z.; Roh, K.; Noel, N. K.; Shapiro, A.; Heremans, P.; Rand, B. P. Mixed Lead–Tin Halide Perovskites for Efficient and Wavelength‐Tunable Near‐Infrared Light‐Emitting Diodes. *Adv. Mater.* **2018,** *31* (3), 1806105, DOI: 10.1002/adma.201806105.
(59) Vashishtha, P.; Halpert, J. E. Field-Driven Ion Migration and Color Instability in Red-Emitting Mixed Halide Perovskite Nanocrystal Light-Emitting Diodes. *Chem. Mater.* **2017,** *29* (14), 5965-5973, DOI: 10.1021/acs.chemmater.7b01609.
(60) Lin, K.; Xing, J.; Quan, L. N.; de Arquer, F. P. G.; Gong, X.; Lu, J.; Xie, L.; Zhao, W.; Zhang, D.; Yan, C.; Li, W.; Liu, X.; Lu, Y.; Kirman, J.; Sargent, E. H.; Xiong, Q.; Wei, Z. Perovskite light-emitting diodes with external quantum efficiency exceeding 20 per cent. *Nature* **2018,** *562* (7726), 245-248, DOI: 10.1038/s41586-018-0575-3.
(61) Shen, X.; Zhang, Y.; Kershaw, S. V.; Li, T.; Wang, C.; Zhang, X.; Wang, W.; Li, D.; Wang, Y.; Lu, M.; Zhang, L.; Sun, C.; Zhao, D.; Qin, G.; Bai, X.; Yu, W. W.; Rogach, A. L. Zn-Alloyed CsPbI3 Nanocrystals for Highly Efficient Perovskite Light-Emitting Devices. *Nano Lett* **2019,** *19* (3), 1552-1559, DOI: 10.1021/acs.nanolett.8b04339.

Graphic for the Table of Contents